npj | climate and atmospheric science

www.nature.com/npjclimatsci

ARTICLE OPEN

Check for updates

Two regimes of inter-basin interactions between the Atlantic and Pacific Oceans on interannual timescales

Jae-Heung Park[1], Sang-Wook Yeh[2]✉, Jong-Seong Kug[1,3]✉, Young-Min Yang[4,5], Hyun-Su Jo[6], Hyo-Jeong Kim[7] and Soon-Il An[1,8]

Understanding the inter-basin interactions between the Atlantic and Pacific Oceans is of great concern due to their substantial global climatic implications. By analyzing observational reanalysis datasets (1948–2020), we found that there are two regimes in Atlantic–Pacific inter-basin interactions: (1) the Pacific-driven regime, and (2) the Atlantic-driven regime. In the Pacific-driven regime before the mid-1980s, the El Niño–Southern Oscillation (ENSO) in winter effectively drives the primary mode of sea surface temperature anomaly (SSTA) in the tropical Atlantic (i.e., North Tropical Atlantic (NTA) mode) in the following spring. The NTA mode has a meridional contrast of SSTA along the Atlantic Intertropical Convergence Zone, similar to the Atlantic Meridional Mode. Whereas, in the Atlantic-driven regime after the mid-1980s, the ENSO effect on the NTA becomes remarkably weaker, so that the NTA mode is featured with a SSTA monopole. Notably, the NTA mode without the meridional contrast of SSTA is capable of modulating an ENSO event with a lag. Our analyses of the latest climate models participating in the Coupled Model Intercomparison Project (CMIP) phases 6 support the hypothesis that the two regimes engendered by the Atlantic–Pacific inter-basin interactions are likely due to natural variability.

npj Climate and Atmospheric Science (2023)6:13 ; https://doi.org/10.1038/s41612-023-00332-3

INTRODUCTION

One important climatic phenomenon that needs to be better understood is the inter-basin interactions in Earth's two largest oceans, the Pacific and Atlantic Oceans, which have enormous impacts on various climate and weather phenomena worldwide[1–4]. Much attention has been paid to the interactions between the Atlantic and the Pacific Oceans, which is crucial for improving the credibility of climate change projections and their associated global impacts[5–8]. The Atlantic–Pacific inter-basin interactions can be specified according to their different timescales. On decadal to interdecadal timescales, Pacific warming (cooling) is able to induce Atlantic warming (warming), whereas Atlantic warming (cooling) possibly causes Pacific cooling (warming)[7–11]. On interannual timescales, the El Niño–Southern Oscillation (ENSO) modulates sea surface temperature anomalies (SSTAs) in the North Tropical Atlantic (NTA) in the following spring to summer via extratropical and tropical atmospheric teleconnections[12–17]. In contrast, the SST variability in the NTA can also modulate an ENSO event in the subsequent boreal winter by altering anomalous low-level zonal winds over the equatorial western Pacific via atmospheric teleconnections[18–21].

The Atlantic–Pacific inter-basin interactions on decadal timescales have been well examined, but those on interannual timescales have not been investigated thoroughly, particularly non-stationary perspectives and their causes. Recent studies have shown that the impact of NTA on the ENSO has become significant since the mid-1980s[17,21,22], as the climatological mean SST in the tropical Atlantic has increased as a result of a positive phase shift of the Atlantic Multi-decadal Oscillation or/and anthropogenic warming[22,23]. The warmer climatological mean SST in the tropical Atlantic promotes an atmospheric response to the SSTA variation, causing an enhanced NTA-ENSO connection. In contrast, the ENSO impact on NTA has weakened since the mid-1980s[17,24].

Therefore, we infer that there are likely two regimes in the Atlantic–Pacific inter-basin interactions on interannual timescales, which has been less examined previously. Understanding the physical mechanisms of the two regimes would help to improve the reliability of climate variability projection in the present-day and future climate. In this study, we examine the physical processes associated with two distinct regimes in the Atlantic–Pacific inter-basin interactions on interannual timescales by analyzing observational datasets and climate models.

RESULTS

Two regimes in the Atlantic–Pacific inter-basin interactions

We first extracted the primary mode of SSTA variability in the tropical Atlantic from spring to summer during 1948–2020 using Extended-Empirical Orthogonal Function (E-EOF) analysis (see "Methods" section), which can identify the spatiotemporal variation of variables of interest. The first E-EOF mode featured the strongest SSTA core off the western North African coast in February–March–April (hereafter, FMA) to April–May–June (AMJ) (Fig. 1a, b). As it moved westward to northeastern South America,

[1]Division of Environmental Science and Engineering, Pohang University of Science and Technology (POSTECH), Pohang, South Korea. [2]Department of Marine Sciences and Convergent Technology, Hanyang University, ERICA, Ansan, Republic of Korea. [3]Institute for Convergence Research and Education in Advanced Technology, Yonsei University, Seoul, South Korea. [4]Key Laboratory of Meteorological Disaster, Ministry of Education (KLME)/Joint International Research Laboratory of Climate and Environment Change (ILCEC)/Collaborative Innovation Center on Forecast and Evaluation of Meteorological Disasters (CIC-FEMD), Nanjing University of Information Science and Technology, Nanjing 210044, China. [5]State Key Laboratory of Numerical Modeling for Atmospheric Sciences and Geophysical Fluid Dynamics, Institute of Atmospheric Physics, Chinese Academy of Sciences, 100029 Beijing, China. [6]Department of Oceanography, Chonnam National University, Gwangju, South Korea. [7]Low-Carbon and Climate Impact Research Centre, School of Energy and Environment, City University of Hong Kong, Tat Chee Ave, Kowloon Tong, Hong Kong, People's Republic of China. [8]Department of Atmospheric Sciences/Irreversible Climate Change Research Center, Yonsei University, Seoul, South Korea. ✉email: swyeh@hanyang.ac.kr; jskug1@gmail.com

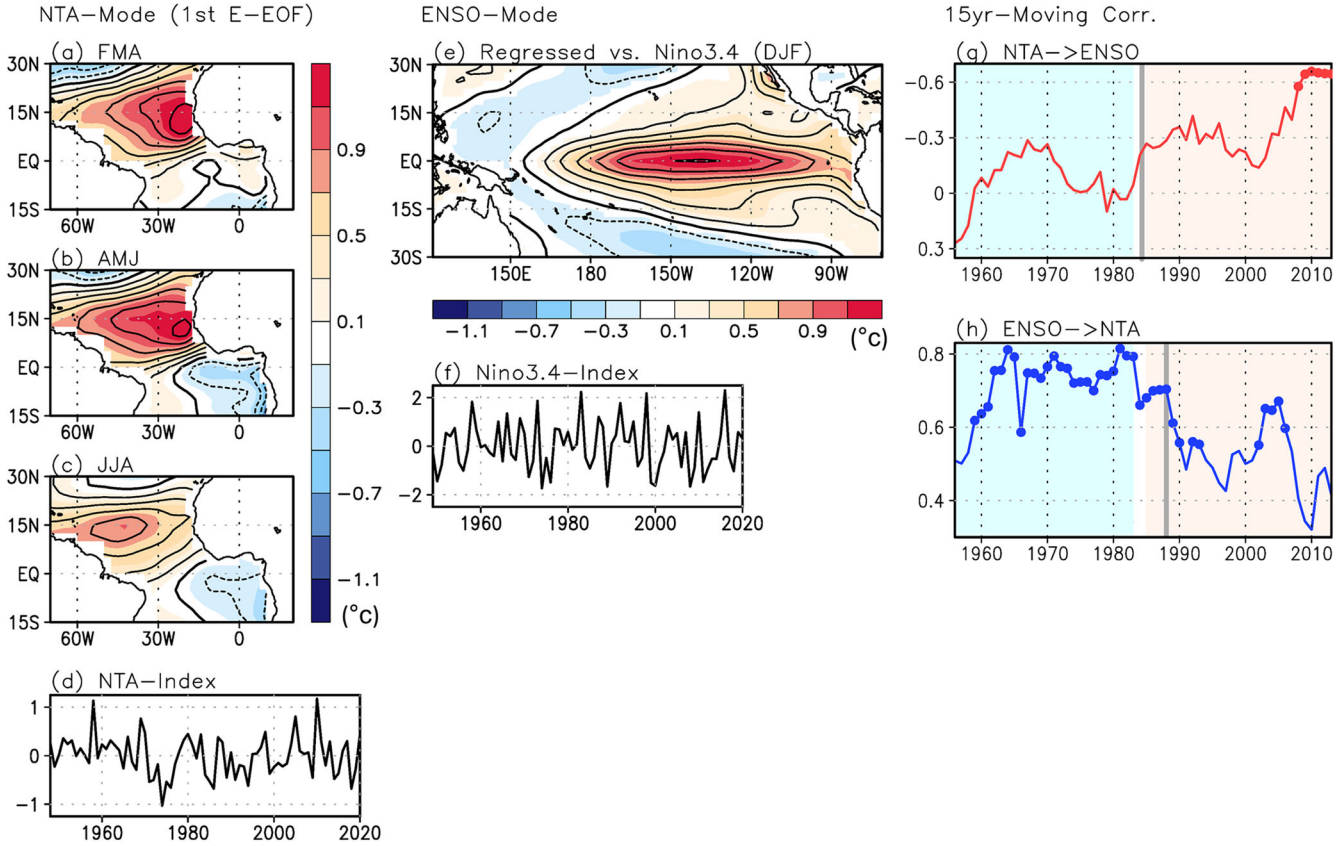

Fig. 1 Relationship between the NTA and the ENSO. a–d The first E-EOF mode of tropical Atlantic SSTAs from spring to summer during 1948–2020. The top three panels indicate (**a**) the FMA mean, (**b**) the AMJ mean, and (**c**) the JJA mean of the SSTAs. The unit is °C and contour interval is 0.2 °C. The color scale is located on the right. **d** shows the principal component (PC) time series of the E-EOF mode. This mode explains almost one-third of the total variability (33.1%) in the tropical Atlantic Ocean. **e**, **f** The ENSO mode: **e** Regressed SSTAs against the Niño-3.4 index in winter (DJF). The unit is °C and contour interval is 0.2 °C. The shading bar locates at the bottom. **f** The Niño-3.4 index are illustrated. **g**, **h** 15-year running lead-lagged correlations between the NTA and ENSO indices during 1948–2020: **g**, **h** indicate NTA-leading-ENSO and ENSO-leading-NTA, respectively. Herein, the Pacific-driven and the Atlantic-driven regimes are shaded in light-blue and light-red, respectively. For **g**, the *y*-axis is reversed to reflect that NTA warming induces a La Niña event. Gray bar in **g** and **h** indicates the regime shift occurred in 1984 for NTA-leading-ENSO correlation and in 1987 for ENSO-leading-NTA correlation, respectively. Herein, dots indicate a 95% confidence level by a Student's *t* test and the Pacific-driven and the Atlantic-driven regimes are shaded in light-blue and light-red, respectively.

the SSTA core decayed with time (Fig. 1c). Additionally, a weak meridional SSTA contrast was observed along the Atlantic intertropical convergence zone (ITCZ) in late spring (AMJ) to summer (June–July–August, JJA) (Fig. 1b, c). This first E-EOF mode explained approximately one-third (33.1%) of the total variability of the tropical Atlantic Ocean SSTA. The first E-EOF principal component (PC) time series (Fig. 1d) was almost identical to the NTA-SSTA index obtained by areal average of SSTA applied in a previous study[18] (correlation coefficient > 0.9; Supplementary Fig. 1). Thus, the first E-EOF mode and its relevant PC time series are here referred to as the NTA mode and the NTA index, respectively. Note that the similar results are obtained when the Hadley Centre Global Sea Ice and Sea Surface Temperature (HadISST) and ECMWF Reanalysis v5 (ERA5) are analyzed (Supplementary Figs. 2–7).

Figure 1e displays the SSTA regressed against the ENSO index, wherein the SSTA warming core is located at 140°W along the equator, exhibiting a typical El Niño structure. The ENSO index is defined as the winter mean (December–January–February, DJF) of the monthly Niño-3.4 index (Fig. 1f). The NTA index corresponds to the spring to summer season, whereas the ENSO index corresponds to the winter season. Thus, a lead-lagged correlation coefficient between the two indices indicates that either the NTA index leads the ENSO index by roughly three seasons (i.e., NTA-leading-ENSO correlation), or the ENSO index leads the NTA index by one season (i.e., ENSO-leading-NTA correlation), implying the strength of either the NTA mode's influence on the ENSO or the ENSO's influence on the NTA mode, respectively.

To reveal non-stationarity in the Atlantic–Pacific inter-basin interactions, we calculated a 15-year running NTA-leading-ENSO (Fig. 1g) and ENSO-leading-NTA correlation (Fig. 1h), respectively. In recent decades the strength of the NTA mode's influence on the ENSO became stronger (Fig. 1g), while the ENSO's influence on the NTA mode became weaker compared to in earlier decades (Fig. 1h). That is, the strength of the NTA mode's influence on the ENSO is inversely related to that of the ENSO's influence on the NTA mode during the entire analysis period. Further analysis indicated that the regime shift change in the NTA–ENSO lead-lagged relationship occurred in the mid-1980s (gray bar in Fig. 1g, h), with a 99% confidence level based on detecting a sequential regime shift (see "Methods" section). This result implies that there are two distinct regimes of the Atlantic–Pacific inter-basin interactions: (1) the Pacific-driven regime before the mid-1980s (i.e., 1948–1983), and (2) the Atlantic-driven regime after the mid-1980s (i.e., 1985–2020).

The Pacific-driven regime versus Atlantic-driven regime in the observations

We performed the E-EOF analysis repeatedly for two subset periods of the Pacific- and Atlantic-driven regimes. The NTA

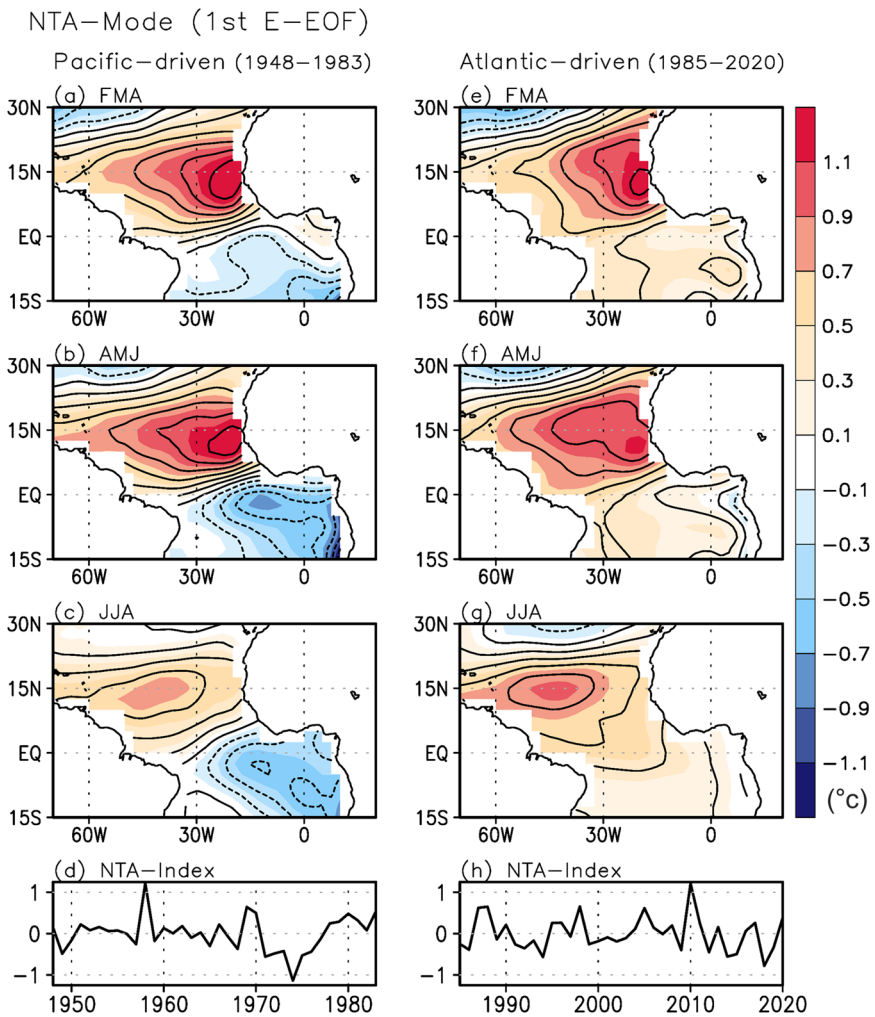

Fig. 2 NTA modes in the different periods. The first E-EOF mode of the Atlantic SSTAs in **a** FMA, **b** AMJ, and **c** JJA during 1948–1983. The unit is °C and contour interval is 0.2 °C. The shading bar locates at the right. **d** The bottom panels show the principal component (PC) time series. **e**–**h** The same as **a**–**d**, but during 1985–2020. The E-EOF modes in each period explain 35.9%, and 36.4% of the total variability, respectively.

modes in the Pacific- (Fig. 2a–d) and Atlantic-driven regimes (Fig. 2e–h) explain 35.9% and 36.4% of the total SST variability, respectively. And, the NTA indices of both regimes (Fig. 2d, h) were highly correlated to the NTA index (Fig. 1d) obtained by using the entire period (correlation coefficients > 0.9). The NTA modes of both regimes shared a common feature in that the SSTA warming center was located near western North Africa. However, there was a significant difference in the equatorial to subtropical South Atlantic. During the Pacific-driven regime, the NTA mode exhibited a dipole-like structure of SSTAs along the Atlantic ITCZ from FMA to JJA (Fig. 2a–c), similar to the Atlantic Meridional Mode (AMM)[25]. In contrast, for the Atlantic-driven period, the meridional contrast of SSTAs weakened as the cool SSTAs in the equatorial to subtropical South Atlantic almost disappeared from FMA to JJA; hence, the SSTA pattern was more likely a monopole (Fig. 2e–g).

Figure 3a–d illustrates the regressed maps of SSTAs, sea level pressure anomalies (SLPAs), anomalous low-level winds, and anomalous precipitation against the NTA index from FMA to August–September–October (ASO) in the Pacific-driven regime (see Supplementary Fig. 8 for the other seasons). In FMA (Fig. 3a), typical El Niño signals appear in the equatorial central-to-eastern Pacific. El Niño generates the Pacific–North America-like teleconnection and, concurrently, appears to be connected to the negative North Atlantic Oscillation (NAO) phase[26–28]. The negative SLPA associated with the southern lobe of the NAO accompanies southwesterly wind anomalies in the NTA. As a result, reduced trade winds caused by the offsetting of the southwesterly wind warm the NTA SSTA with weakened latent heat released from the oceanic surface. At the same time, the El Niño modulates the tropical atmospheric teleconnection (i.e., the Walker circulation) by maintaining its strength until late spring (AMJ; Fig. 3b). This generates low-level easterly wind anomalies over the eastern equatorial Atlantic, inducing SSTA cooling in the equatorial Atlantic by enhancing evaporative cooling. In short, El Niño can explain the formation of both NTA warming and equatorial cooling in spring to summer with local atmosphere–ocean feedback over the equatorial Atlantic Ocean. This resembles the AMM[25].

Through spring to summer (Fig. 3a–c), the NTA-SSTA warming accompanies enhanced precipitation in situ, while the equatorial to subtropical Atlantic SSTA cooling induces reduced precipitation there. According to a previous modeling study by Jiang and Li[29], the atmospheric responses to the opposite precipitation anomalies over the tropical Atlantic offset their effects toward the tropical Pacific. Consequently, the NTA mode does not influence the SST variability in the equatorial Pacific in the following seasons during the Pacific-driven regime (Fig. 3d).

We analyzed the evolution of the NTA mode in the Atlantic-driven regime using a similar approach (Fig. 3e–h). In contrast to

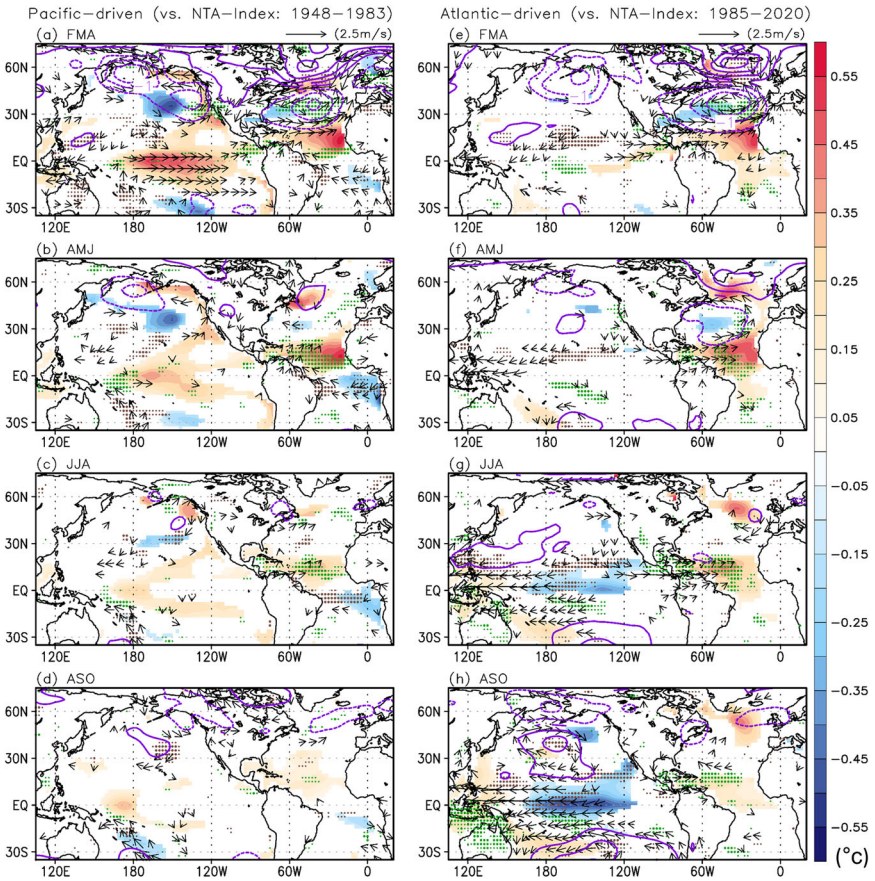

Fig. 3 Pacific- and Atlantic-driven interactions. a Regressed SSTAs (°C, shading bar at right), sea level pressure anomalies (contour, 0.5 hPa), low-level wind anomalies (vector, at 850 hPa), and precipitation anomalies (dots, green and brown for positive and negative) in FMA against the NTA index during the Pacific-driven regime (1948–1983). **b**–**d** Same as **a**, but in AMJ, JJA, ASO. The SSTAs, winds, and precipitation reflect a 95% confidence level by a Student's *t* test. **e**–**h** The same as **a**–**d**, but for the Atlantic-driven regime (1985–2020).

the Pacific-driven regime, the El Niño signals are significantly weaker during FMA (Fig. 3e), and the Pacific North America-like atmospheric teleconnection as well as the Walker circulation are not as strong. Instead, the NAO-like SLPA, which can be considered as an internal atmospheric variability[30], is well-defined over the North Atlantic until AMJ (Fig. 3f; see also MJJ in Supplementary Fig. 8). Therefore, the NTA mode is largely affected by the NAO[31,32] during the Atlantic-driven regime. The NTA warming is expanded to the equatorial southern Atlantic from FMA to AMJ with the 95% confidence level during the Atlantic-driven period. It is important to note that during the Pacific-driven period, the NTA warming is limited in the northern Atlantic with a cool SSTA over the Benguela region which grows along the equatorial Atlantic from spring to summer as the time progresses (Fig. 3a–c) with the local ocean–atmosphere feedback initiated by the previous ENSO. As a result, the NTA mode has a SSTA monopole in the tropical Atlantic (15°S–30°N) in this regime (Fig. 3e–g).

With the SSTA monopole, anomalous precipitation is enhanced over the tropical Atlantic in AMJ to JJA (Fig. 3f, g), which is different from the precipitation contrast along the Atlantic ITCZ in the Pacific-driven regime (Fig. 3b, c). The enhanced precipitation over the tropical Atlantic generates the Rossby wave energy propagation toward the subtropical North Pacific, inducing northerly wind anomalies over the subtropical North Pacific, which in turn brings negative precipitation anomalies there during AMJ and JJA[29] (Fig. 3f, g). Together with the Walker circulation modulated by the enhanced precipitation over the tropical Atlantic[18], easterly wind anomalies are induced over the western equatorial Pacific (Fig. 3g, h), promoting La Niña development (Fig. 3h).

Physical processes in the natural variability of Atlantic–Pacific inter-basin interactions

We hypothesize that the two regimes engendered by the Atlantic–Pacific inter-basin interactions are likely due to natural variability. Understanding which processes contribute to the natural variability of the Atlantic–Pacific inter-basin interactions is meaningful. Because the NAO, which is known to be due to internal climate variability[30,33,34], mainly contributes to the formation of the NTA mode[31,32], first we examined changes in NAO variability. We found that the NAO-like atmospheric variability in winter to spring has become abruptly enhanced since the mid-1980s (15.5% increase, from 3.96 (std: 0.26) in 1948–1983 to 4.57 hPa (std: 0.40) in 1985–2020) (Fig. 4a). This increased NAO variability maintains the NTA mode's intensity, which also helps to induce a monopole structure of SSTAs and precipitation, instead of a dipole structure of SSTAs and precipitation induced by the ENSO teleconnection. Although the decadal modulation of the NAO variability cannot fully explain the change in the NTA mode, the enhanced NAO variability after the mid-1980s contributes to some extent the modulation of the NTA mode.

Of additional note is the change in the climatological precipitation contrast between the Atlantic and Pacific Oceans on decadal timescales. There has been a continuous increase in the climatological mean precipitation in the tropical Atlantic (10.3%, 5.23 to 5.77 mm/day), while in contrast, the mean

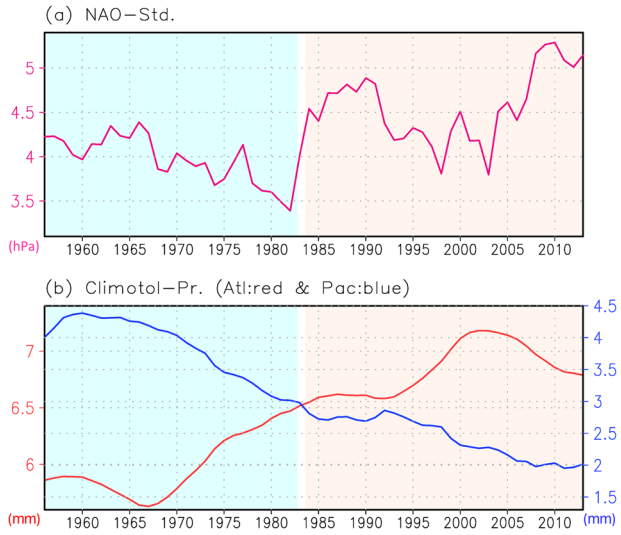

Fig. 4 Observed changes in climatology over 1948–2020. **a** 15-year running standard deviation of the NAO index in spring (FMA). **b** Filtered mean of climatological precipitation in the tropical Atlantic (0–80°W, 5°S–5°N, FMA, red line, left axis) and Pacific (120–170°W, 5°S–5°N, DJF, blue line, right axis), smoothed by the repeated application of a triangular filter, equivalent to a $(2 \times 7 + 1$, 15-year) point binomial filter.

precipitation in the tropical Pacific has decreased significantly (−35.6%, 3.79 to 2.44 mm/day) (Fig. 4b). It is known that when a low-level convergence anomaly occurs over a higher climatological mean low-level convergence area, the atmospheric response can be amplified through the moisture convergence feedback[35]. For example, the increase in the climatological mean precipitation (i.e., moisture) in the tropical Atlantic is related to the strengthened atmospheric teleconnection from the tropical Atlantic and the weakened atmospheric teleconnection from the tropical Pacific, and vice versa.

Atlantic–Pacific inter-basin interactions in CMIP6 climate models

We speculate that climate models struggle to simulate the two-way interactions between the Atlantic and the Pacific compared to observations. There are several potential explanations for this notion. For instance, it has been reported that climate models fail to reproduce the observed mean state[36], which includes a Pacific cold tongue[37,38], zonal SST contrast in the equatorial Atlantic[39], and the ITCZ location[40,41]. Furthermore, some climate models exhibit discrepancies in atmosphere–ocean coupled processes compared to the observation[42], including air-sea coupling strength in two basins, ENSO phase locking[19], and ENSO diversity[43–46]. Additionally, simulations of the internal climate variability, in terms of its intensity and frequency, vary among climate models[47,48]. However, we cannot exclude the possibility that the observed relationship of two-way interactions, which is obtained from a relatively short period of dataset, might be accidental.

Nonetheless, it would be beneficial to investigate the Atlantic–Pacific inter-basin interaction in climate models to examine whether it is a natural climate variability or not. We analyzed the pre-industrial runs from 19 climate models participating in the Coupled Model Intercomparison Project (CMIP) phases 6, respectively (Table 1 in the "Methods" section). Following the methodology applied to the observation, the ENSO index was obtained as a winter mean (DJF) Niño-3.4 index, and the NTA index was defined as the PC time series of the 1st E-EOF of tropical Atlantic SSTA in each climate model. First, we evaluated

Table 1. Pre-industrial simulations used in this study.

CMIP6	Period (year)
ACCESS-CM2	500
ACCESS-ESM1-5	900
CanESM5	1000
CanESM5-CanOE	500
CESM2	1200
CESM2-WACCM	500
CESM2-WACCM-FV2	500
E3SM-1-0	500
INM-CM4-8	530
INM-CM5-0	1200
MIROC6	500
MIROC-ES2L	500
MPI-ESM-1-2-HAM	780
MPI-ESM1-2-HR	500
MPI-ESM1-2-LR	1000
MRI-ESM2-0	700
NorCPM1	500
NorESM2-LM	500
NorESM2-MM	500

19 CMIP5 climate models and their simulated duration.

the fidelity of the ENSO pattern simulation in each climate model based on the regressed SSTA pattern against the NINO3.4 SST index. It is found that the ENSO pattern correlations between the observation and CMIP6 climate models are significantly high, greater than 0.9 except for a few models (Fig. 5a), indicating that most CMIP6 models are capable of simulating ENSO pattern reasonably. Similarly, it is also evaluated how well CMIP6 climate models simulate the observed evolutionary features of the NTA mode (Fig. 5b and see also Supplementary Fig. 9). Unlike the ENSO patterns, the patterns of the NTA mode are very diverse among climate models. Based on this result (Fig. 5b), we selected 8 climate models of which pattern correlations of the 1st E-EOF mode with the observation are greater than 0.8. We note that all results are not significantly changed when the criterion is replaced to 0.7. Then, a 15-year running NTA-leading-ENSO correlation is defined to represent the strength of the NTA effect on ENSO on decadal timescales, and the periods of the highest and lowest 20% of those correlations are selected in the entire simulation period of pre-industrial runs from 8 climate models.

Figure 5c, d illustrates the ensemble mean of the NTA mode during the periods of strong and weak NTA effect on ENSO, respectively (see also Supplementary Fig. 10). The ensemble mean of the 1st E-EOF mode has a meridional SSTA dipole during the period of weak NTA effect on ENSO, whereas it is less clear during the period of strong NTA effect on ENSO, simlar to the observation (Fig. 2). Next, the ensemble mean of the SSTA regressed against the NTA index was examined (Supplementary Fig. 11). While there are some discrepancies compared with the observation such as too strong previous El Nino with long persistency, it is found that the SSTA contrast in the equatorial Atlantic Ocean is a bit weaker from spring to summer during the period of strong NTA effect on ENSO than that during the period of weak NTA effect on ENSO although it is not significant. Indeed, during the period of strong NTA effect on ENSO, the previous El Nino is weaker with less persistency and the NTA warming is able to lead a La Nina development like the observation. These results may support the notion that the two regimes engendered by the Atlantic–Pacific inter-basin interactions are likely due to natural variability.

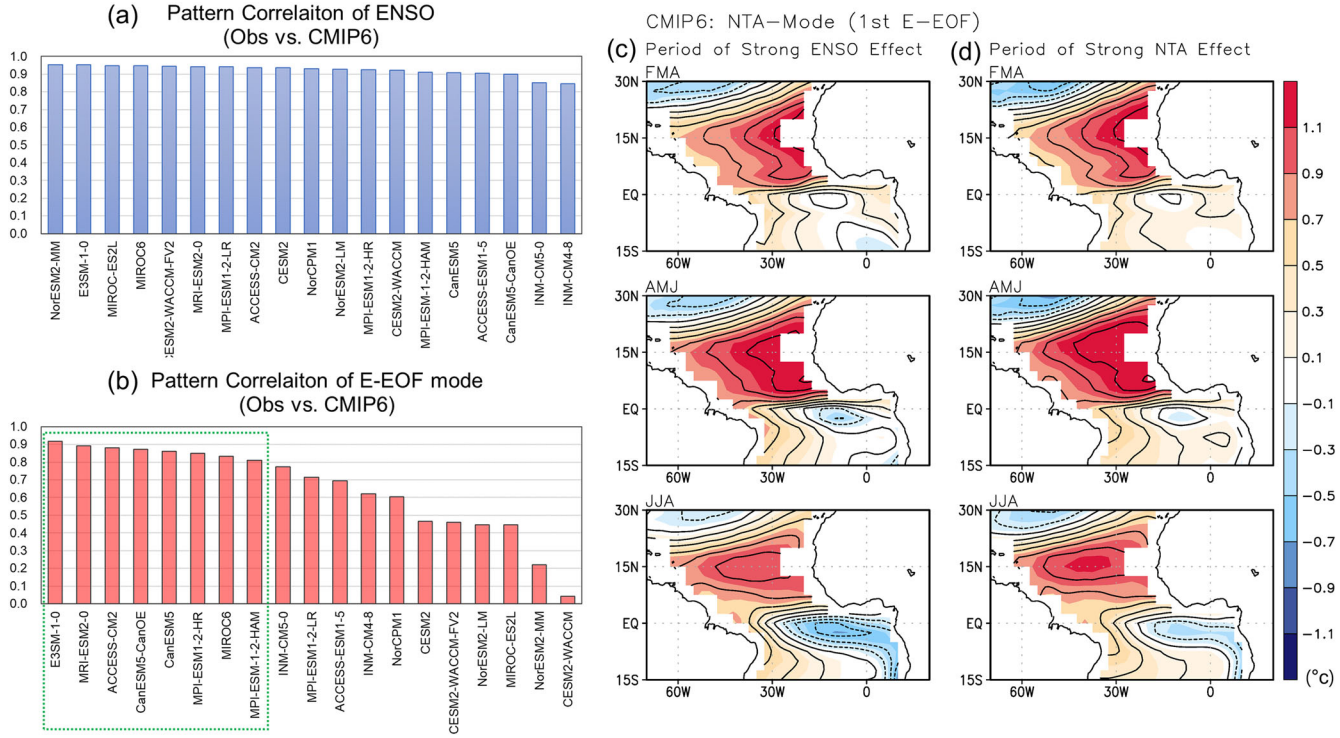

Fig. 5 Patterns of ENSO and NTA mode in CMIP6 climate models. a Pattern correlation coefficients between the observation and CMIP6 climate model's ENSO. Herein the ENSO patterns of both observations (Fig. 1e) and climate models are obtained by regressing SSTA onto Nino-3.4 index in boreal winter (December to February). **b** Pattern correlation coefficients of the 1st E-EOF mode between the observation (Fig. 1a–c) and CMIP6 climate models. **c** The 8-model ensemble mean of the first E-EOF mode of the Atlantic SSTAs in (top) FMA, (middle) AMJ, and (bottom) JJA during the period of weak NTA effect. The unit is °C and contour interval is 0.2 °C. The shading bar locates at the right. (right). **d** The same as **c**, but during the strong period of NTA effect.

DISCUSSION

Thus far in this study we have investigated observed interdecadal modulation in the lead-lagged relationship between NTA and ENSO on interannual timescales over 1948–2020, and have demonstrated that there are two different regimes of the Pacific–Atlantic inter-basin interactions, driven by the Pacific and the Atlantic, respectively. Figure 6 is a schematic diagram illustrating the Pacific- and Atlantic-driven inter-basin interactions. For the Pacific-driven regime (Fig. 6a), the ENSO generates atmospheric teleconnection via both extratropics and tropics, which contributes to the AMM-like SSTA dipole along the Atlantic ITCZ in spring to summer. In this situation, precipitation contrast is introduced along the ITCZ, in which induced opposite atmospheric responses offset each other in the tropical Pacific. Thus, the influence of the tropical Atlantic on the tropical Pacific is reduced in the Pacific-driven regime. In contrast, during the Atlantic-driven regime (Fig. 6b) the ENSO influence on the tropical Atlantic is weak. At that time, the internal atmospheric variability in the Atlantic (i.e., NAO-like atmospheric circulation) plays an important role in forming the monopole SSTA variability. Such a monopole SSTA accompanies the overall enhancement of precipitation in the tropical Atlantic, which effectively modulates zonal winds. Thus, tropical Atlantic signals are well-transported to the tropical Pacific, modulating ENSO events. It is noteworthy that the absolute ENSO-leading-NTA correlation is mostly greater than the NTA-leading-ENSO correlation during the entire analyzed period (Fig. 1g, h), implying that the Pacific more easily influences the Atlantic than vice versa.

As to the future projection of the Atlantic–Pacific inter-basin interactions, a recent study argued that the ENSO effect on the NTA will be strengthened[49] due to the eastward displacement of the ENSO action center and following atmospheric teleconnections. Additionally, it is suggested that the NTA effect on the ENSO will be decreased as the SSTs in the tropical Pacific increase faster than in the tropical Atlantic[20]. Both results imply the possibility that the Pacific-driven regime will be favored in the future. However, it should be noted that most climate models still weakly simulate the Atlantic–Pacific inter-basin interactions and there are unknown factors involved. Therefore, conclusions regarding their future changes should be approached with caution.

METHODS

Reanalysis datasets

For observational reanalysis data, we used the monthly dataset of the (U.S. NOAA) National Center for Environmental Prediction Reanalysis 1 (NCEP-R1), which is an assimilated dataset that uses a state-of-the-art analysis and forecast system[50]. This sea level pressure, wind, and precipitation dataset has been widely used due to its reliability as well as to its relatively long record, spanning from 1948 to the present. For SSTs, we used NOAA's Extended Reconstruction Sea Surface Temperature version 5 (ERSSTv5)[51], which is a global monthly SST dataset derived from NOAA's International Comprehensive Ocean-Atmosphere Dataset (ICOADS), available from 1854 to the present. The analysis period in this study was from 1948 to 2020. Additionally, HadISST[52] (1948–2020) and ERA5[53] reanalysis dataset (1950–2020) is also used to test the robustness of the results.

Extended empirical orthogonal functions (E-EOFs)

The extended empirical orthogonal functions (E-EOFs) constitute an extension of the traditional EOF technique to deal with spatial as well as temporal correlations observed in weather/climate data. The method was first introduced by Weare and Nasstrom[54].

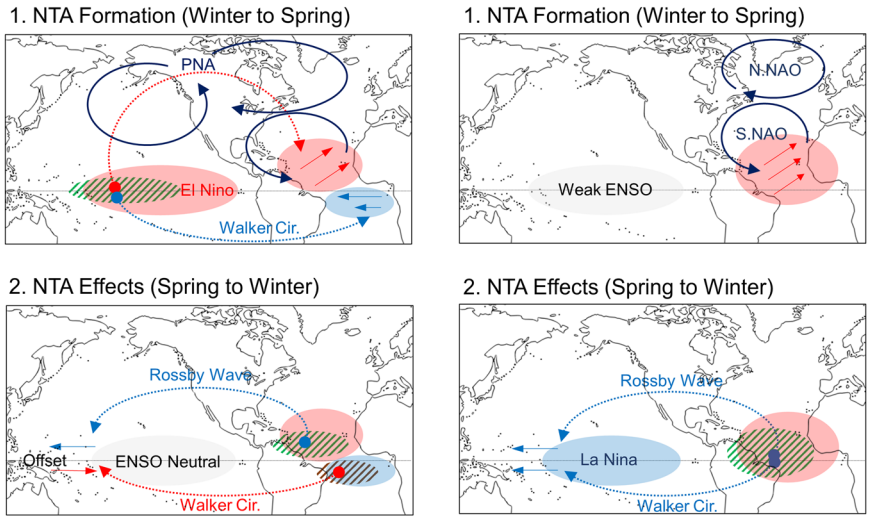

Fig. 6 A schematic diagram of the two regimes of Atlantic–Pacific interaction. a The NTA mode formation during winter to late spring, and its effect on the tropical Pacific during late spring to subsequent winter in the Pacific-driven regime (1948–1983). The red, blue, and gray shadings indicate SSTA warming, cooling, and normal conditions. Red and blue dotted arrows illustrate atmospheric teleconnections that results in warming and cooling of the underlying SSTAs, respectively. Dark blue solid arrows indicate atmospheric circulation at low levels in association with PNA and NAO. The straight red and blue arrows indicate anomalous low-level winds. The green and brown hatched lines mean enhanced and reduced precipitation. **b** is similar to **a**, but in the Atlantic-driven regime (1985–2020).

The E-EOF analysis allows for the time-sequence evolution of SSTAs in the analyzed domain. In this study the input vectors are composed of the FMA–AMJ–JJA SSTA mean fields of 73-year (1948–2020) in the tropical Atlantic.

Sequential regime shift detection

To detect regime shift, we utilized the sequential regime shift detection method developed by Sergei and Overland[55]. The main advantage of this method is its ability to process data in real time, signaling the emergence of a potential shift and measuring changing confidence in the evidence for a shift as new data arrive. The method does not require initial visual inspection of a time series or an a priori hypothesis about the timing of the shift. It can process time series with multiple shifts, and handle input regardless of whether the data are presented in the form of anomalies or absolute values. The method is applied based on a sequential *t*-test that can signal the possibility of a regime shift in real time by automatically detecting statistically significant shifts in the mean level and the magnitude of fluctuations in time series. The relevant software can be downloaded from https://www.beringclimate.noaa.gov/regimes/. We applied this method to the lead-lagged correlation coefficients between the NTA and the ENSO indices (Fig. 1g, h), and confirmed, at the 99% confidence level, that a regime shift occurred in the mid-1980s (1984 for the NTA's influence on the ENSO and 1987 for the ENSO's influence on the NTA).

Pre-industrial simulations of CMIP6 climate model

We used SSTs in the pre-industrial runs of 19 CMIP6 climate models to investigate the basic interactions between the Atlantic and the Pacific; the resulting model names and durations are listed in Table 1. The horizontal resolution was interpolated into 2.5° (longitude) × 2.5° (latitude).

DATA AVAILABILITY

ERSST v5, HadISST, and ERA5 can be downloaded from following URL: https://www.esrl.noaa.gov/psd/data/data.php, https://www.metoffice.gov.uk/hadobs/hadisst/data/download.html, https://cds.climate.copernicus.eu/cdsapp#!/search?text=ERA5%20back%20extension&type=dataset, respectively. CMIP6 can be downloaded from https://esgf-node.llnl.gov/projects/cmip6/.

CODE AVAILABILITY

Codes used in the manuscript are available upon reasonable requests from J.-H.P. (jhp11010@gmail.com).

Received: 16 February 2022; Accepted: 8 February 2023;
Published online: 22 February 2023

REFERENCES

1. McCabe, G. J., Palecki, M. A. & Betancourt, J. L. Pacific and Atlantic Ocean influences on multidecadal drought frequency in the United States. *Proc. Natl Acad. Sci. USA* **101**, 4136 LP–4134141 (2004).
2. Bell, G. D. & Chelliah, M. Leading tropical modes associated with interannual and multidecadal fluctuations in north Atlantic hurricane activity. *J. Clim.* **19**, 590–612 (2006).
3. Cai, W. et al. Pantropical climate interactions. *Science* **363**, eaav4236 (2019).
4. Wang, C. Three-ocean interactions and climate variability: a review and perspective. *Clim. Dyn.* **53**, 5119–5136 (2019).
5. Kosaka, Y. & Xie, S.-P. Recent global-warming hiatus tied to equatorial Pacific surface cooling. *Nature* **501**, 403–407 (2013).
6. England, M. H. et al. Recent intensification of wind-driven circulation in the Pacific and the ongoing warming hiatus. *Nat. Clim. Chang.* **4**, 222–227 (2014).
7. McGregor, S. et al. Recent walker circulation strengthening and pacific cooling amplified by atlantic warming. *Nat. Clim. Chang.* **4**, 888–892 (2014).
8. Li, X., Xie, S. P., Gille, S. T. & Yoo, C. Atlantic-induced pan-tropical climate change over the past three decades. *Nat. Clim. Chang.* **6**, 275–279 (2016).
9. Latif, M. & Grötzner, A. The equatorial Atlantic oscillation and its response to ENSO. *Clim. Dyn.* **16**, 213–218 (2000).
10. Meehl, G. A., Hu, A., Santer, B. D. & Xie, S. P. Contribution of the Interdecadal Pacific Oscillation to twentieth-century global surface temperature trends. *Nat. Clim. Chang.* **6**, 1005–1008 (2016).
11. Levine, A. F. Z., McPhaden, M. J. & Frierson, D. M. W. The impact of the AMO on multidecadal ENSO variability. *Geophys. Res. Lett.* **44**, 3877–3886 (2017).
12. Enfield, D. B. & Mayer, D. A. Tropical atlantic sea surface temperature variability and its relation to El Niño-Southern Oscillation. *J. Geophys. Res. C. Ocean.* **102**, 929–945 (1997).
13. Klein, S. A., Soden, B. J. & Lau, N.-C. Remote sea surface temperature variations during ENSO: evidence for a tropical atmospheric bridge. *J. Clim.* **12**, 917–932 (1999).

14. Giannini, A., Cane, M. A. & Kushnir, Y. Interdecadal changes in the ENSO teleconnection to the Caribbean region and the North Atlantic Oscillation. *J. Clim.* **14**, 2867–2879 (2001).
15. Chiang, J. C. H. & Sobel, A. H. Tropical tropospheric temperature variations caused by ENSO and their influence on the remote tropical climate. *J. Clim.* **15**, 2616–2631 (2002).
16. Mélice, J. L. & Servain, J. The tropical Atlantic meridional SST gradient index and its relationships with the SOI, NAO and Southern Ocean. *Clim. Dyn.* **20**, 447–464 (2003).
17. Park, J.-H. & Li, T. Interdecadal modulation of El Niño–tropical North Atlantic teleconnection by the Atlantic multi-decadal oscillation. *Clim. Dyn.* **52**, 5345–5360 (2019).
18. Ham, Y. G., Kug, J. S., Park, J. Y. & Jin, F. F. Sea surface temperature in the north tropical Atlantic as a trigger for El Niño/Southern Oscillation events. *Nat. Geosci.* **6**, 112–116 (2013).
19. Ham, Y. G. & Kug, J. S. Role of north tropical atlantic SST on the ENSO simulated using CMIP3 and CMIP5 models. *Clim. Dyn.* **45**, 3103–3117 (2015).
20. Choi, J. Y., Ham, Y. G. & McGregor, S. Atlantic-Pacific SST gradient change responsible for the weakening of North Tropical Atlantic-ENSO relationship due to global warming. *Geophys. Res. Lett.* 7574–7582 https://doi.org/10.1029/2019GL082804 (2019).
21. Park, J.-H. et al. Role of the climatological North Pacific High in the North Tropical Atlantic–ENSO connection. *J. Clim.* **35**, 3215–3226 (2022).
22. Wang, L., Yu, J.-Y. & Paek, H. Enhanced biennial variability in the Pacific due to Atlantic capacitor effect. *Nat. Commun.* **8**, 14887 (2017).
23. Park, J. H., Li, T., Yeh, S. W. & Kim, H. Effect of recent Atlantic warming in strengthening Atlantic–Pacific teleconnection on interannual timescale via enhanced connection with the pacific meridional mode. *Clim. Dyn.* **53**, 371–387 (2019).
24. Zhang, W., Jiang, F., Stuecker, M. F., Jin, F.-F. & Timmermann, A. Spurious North Tropical Atlantic precursors to El Niño. *Nat. Commun.* **12**, 4–11 (2021).
25. Chiang, J. C. H. & Vimont, D. J. Analogous Pacific and Atlantic meridional modes of tropical atmosphere–ocean variability. *J. Clim.* **17**, 4143–4158 (2004).
26. Mathieu, P.-P., Sutton, R. T., Dong, B. & Collins, M. Predictability of winter climate over the North Atlantic European region during ENSO events. *J. Clim.* **17**, 1953–1974 (2004).
27. Brönnimann, S., Xoplaki, E., Casty, C., Pauling, A. & Luterbacher, J. ENSO influence on Europe during the last centuries. *Clim. Dyn.* **28**, 181–197 (2007).
28. Brönnimann, S. Impact of El Niño–Southern Oscillation on European climate. *Rev. Geophys*. **45**, RG3003 (2007).
29. Jiang, L. & Li, T. Impacts of Tropical North Atlantic and Equatorial Atlantic SST anomalies on ENSO. *J. Clim*. 1–58 https://doi.org/10.1175/JCLI-D-20-0835.1 (2021).
30. Barnett, T. P. Variations in near-global sea level pressure. *J. Atmos. Sci.* **42**, 478–501 (1985).
31. Okumura, Y., Xie, S.-P., Numaguti, A. & Tanimoto, Y. Tropical Atlantic air-sea interaction and its influence on the NAO. *Geophys. Res. Lett.* **28**, 1507–1510 (2001).
32. Huang, B. & Shukla, J. Ocean-atmosphere interactions in the tropical and subtropical Atlantic Ocean. *J. Clim.* **18**, 1652–1672 (2005).
33. Scaife, A. A. et al. Skillful long-range prediction of European and North American winters. *Geophys. Res. Lett.* **41**, 2514–2519 (2014).
34. Greatbatch, R. J. The North Atlantic Oscillation. *Stoch. Environ. Res. Risk Assess.* **14**, 213–242 (2000).
35. Zebiak, S. E. Atmospheric convergence feedback in a simple model for El Ni?o. *Mon. Weather Rev.* **114**, 1263–1271 (1986).
36. Wang, C., Zhang, L., Lee, S. K., Wu, L. & Mechoso, C. R. A global perspective on CMIP5 climate model biases. *Nat. Clim. Chang.* **4**, 201–205 (2014).
37. Li, G. & Xie, S.-P. Origins of tropical-wide SST biases in CMIP multi-model ensembles. *Geophys. Res. Lett.* **39**, L22703 (2012).
38. Li, G. & Xie, S.-P. Tropical biases in CMIP5 multimodel ensemble: the excessive equatorial Pacific cold tongue and double ITCZ problems. *J. Clim.* **27**, 1765–1780 (2014).
39. Richter, I., Xie, S. P., Behera, S. K., Doi, T. & Masumoto, Y. Equatorial Atlantic variability and its relation to mean state biases in CMIP5. *Clim. Dyn.* **42**, 171–188 (2014).
40. Tian, B. & Dong, X. The double-ITCZ bias in CMIP3, CMIP5, and CMIP6 models based on annual mean precipitation. *Geophys. Res. Lett.* **47**, e2020GL087232 (2020).
41. Oueslati, B. & Bellon, G. The double ITCZ bias in CMIP5 models: interaction between SST, large-scale circulation and precipitation. *Clim. Dyn.* **44**, 585–607 (2015).
42. Park, J.-H. et al. Role of the climatological intertropical convergence zone in the seasonal footprinting mechanism of El Niño–Southern Oscillation. *J. Clim.* **34**, 5243–5256 (2021).
43. Kao, H. Y. & Yu, J. Y. Contrasting Eastern-Pacific and Central-Pacific types of ENSO. *J. Clim.* **22**, 615–632 (2009).
44. Yeh, S.-W. et al. El Niño in a changing climate. *Nature* **461**, 511–514 (2009).
45. Kug, J. S., Jin, F. F. & An, S. Two types of El Niño events: cold tongue El Niño and warm pool El Niño. *J. Clim.* **22**, 1499–1515 (2009).
46. Ashok, K., Behera, S. K., Rao, S. A., Weng, H. & Yamagata, T. El Niño Modoki and its possible teleconnection. *J. Geophys. Res. Ocean.* **112**, 1–27 (2007).
47. Ham, Y.-G. & Kug, J.-S. How well do current climate models simulate two types of El Nino? *Clim. Dyn.* **39**, 383–398 (2012).
48. Jia, F. et al. Weakening Atlantic Niño–Pacific connection under greenhouse warming. *Sci. Adv.* **5**, eaax4111 (2019).
49. Yun, Y. et al. Greenhouse warming intensifies north tropical Atlantic climate variability. *Sci. Adv.* **7**, eabg9690 (2021).
50. Kistler, R. et al. The NCEP-NCAR 50-year reanalysis: monthly means CD-ROM and documentation. *Bull. Am. Meteorol. Soc.* **82**, 247–267 (2001).
51. Huang, B. et al. Extended reconstructed sea surface temperature, version 5 (ERSSTv5): upgrades, validations, and intercomparisons. *J. Clim.* **30**, 8179–8205 (2017).
52. Rayner, N. A. et al. Global analyses of sea surface temperature, sea ice, and night marine air temperature since the late nineteenth century. *J. Geophys. Res. Atmos.* **108**, 4407 (2003).
53. Hersbach, H. et al. The ERA5 global reanalysis. *Q. J. R. Meteorol. Soc.* **146**, 1999–2049 (2020).
54. Weare, B. C. & Nasstrom, J. S. Examples of extended empirical orthogonal function analyses. *Mon. Weather Rev.* **110**, 481–485 (1982).
55. Rodionov, S. & Overland, J. E. Application of a sequential regime shift detection method to the Bering Sea ecosystem. *ICES J. Mar. Sci.* **62**, 328–332 (2005).

ACKNOWLEDGEMENTS

We appreciate the constructive comments and suggestions provided by the anonymous reviewers and editors. This work was supported by a National Research Foundation (NRF) of Korea grant funded by the Korean government (MSIT) (NRF-2020R1C1C1006569). S.-W.Y. was supported by the National Research Foundation of Korea (NRF) grant (NRF-2018R1A5A1024958). This work was also supported by the National Research Foundation of Korea (NRF) grant funded by the Korean government (NRF-2022R1A3B1077622).

AUTHOR CONTRIBUTIONS

J.-H.P. conceived idea and prepared figures. J.-H.P., S.-W.Y. and J.-S.K. wrote the manuscript. All the authors discussed the study results and reviewed the manuscript.

COMPETING INTERESTS

The authors declare no competing interests.

ADDITIONAL INFORMATION

Supplementary information The online version contains supplementary material available at https://doi.org/10.1038/s41612-023-00332-3.

Correspondence and requests for materials should be addressed to Sang-Wook Yeh or Jong-Seong Kug.

Reprints and permission information is available at http://www.nature.com/reprints

Publisher's note Springer Nature remains neutral with regard to jurisdictional claims in published maps and institutional affiliations.